COMPENSATION STRATEGIES FOR ROBOTIC MOTION ERRORS FOR ADDITIVE MANUFACTURING (AM)

Yashwanth K. Bandari[1,*], Thomas O.H. Charrett[2], Florent Michel[1], Jialuo Ding[1], Stewart W. Williams[1], Ralph P. Tatam[2]

[1]Welding Engineering and Laser Processing Centre (WELPC), Cranfield University, Cranfield
[2]Centre for Engineering Photonics, Cranfield University, Cranfield
MK43 0AL, United Kingdom
*y.k.bandari@cranfield.ac.uk

Abstract

It is desirable to utilise a robotic approach in additive manufacturing as Computer Numerical Control (CNC) is expensive and it has high maintenance costs. A robotic approach is relatively inexpensive compared to CNC and can provide much more flexibility, enabling a variety of configurations and easier parallel processing. However, robots struggle to achieve high positioning accuracy and are more prone to disturbances from the process forces. This paper attempts to characterise the robot position and velocity errors, which depend on the build strategy deployed, using a laser speckle correlation sensor to measure the robotic motion. An assessment has been done as to whether these errors would cause any problem in additive manufacturing techniques, where the test parts were built using the Wire+Arc Additive Manufacture (WAAM) technique. Finally, different compensation strategies are discussed to counter the robotic errors and a reduction of 3 mm in top surface profile irregularity by varying the wire feed speed (WFS) during the path has been demonstrated.

Keywords: Robotics, Additive Manufacture, Oscillation Strategy, Lasers, Speckle Correlation, Odometry

1. Introduction

Additive Manufacturing (AM), also known as 3D-printing, has gained more traction over the past 30 years in the manufacturing sector, particularly in producing prototypes and models. The advantages of AM range from producing parts without the use of fixtures, cutting tools, coolants to cutting down production cost and lead time by a significant margin, compared to the traditional processes such as machining and stamping. Zhang et. al [1] give an analysis and future insights into the AM technology and market for various industry sectors, including aerospace, automotive, medical, and electronics. Furthermore, Wohler's 2016 Report on Additive Manufacturing gave a comprehensive assessment and evaluation of the AM industry [2]. According to it, the AM industry has grown by $1 billion for two years in a row to a total of $5,165 billion. Despite some challenges with the AM industry, growth was particularly seen in two distinct and seemingly opposite sectors: industrial metal additive manufacturing and desktop 3D printers. In 2013, sale of metal 3D printers went up by a massive 74% and in 2015, the interest in metal 3D printers was still quite high, with sales up another 45%.

AM of metre scale parts requires direct feed processes such as blown powder or wire feed combine with lasers or arcs and the overall system can be configured using either a robotic or Computer Numerical Control (CNC) gantry system [3]. There are many factors that determine which of these is best; both robotic and CNC options have been evaluated in [3]. Production implementations of robots in the aerospace industry have been active for many years and with varying degrees of success [4]. For building large scale aerospace components, robots on rails will have advantage over the traditional CNC machines, due to wider working envelope.

Figure 1 shows one such set up at Cranfield University. Robots offer benefits in both cost and application flexibility. However, they struggle to achieve high positioning accuracy level, being limited to 0.5-2 mm [5] and at the same time are more prone to disturbances from the process forces.
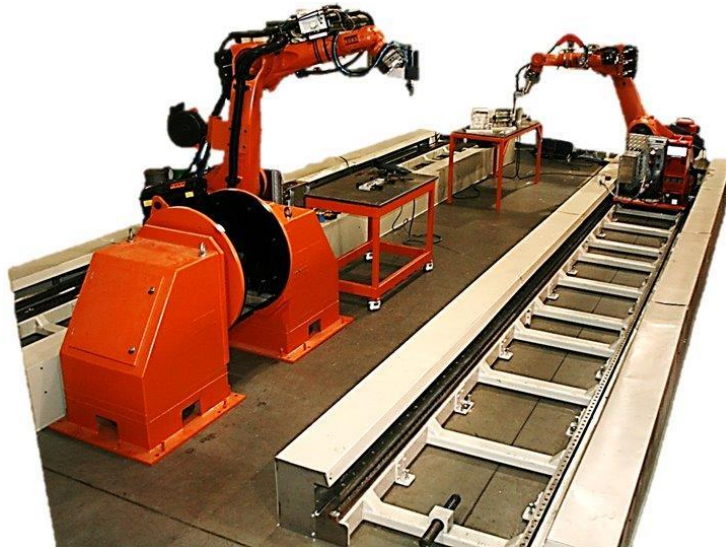

Figure 1 Twin robot system on rails

This paper aims to characterise the robotic position and velocity errors using a speckle correlation, and evaluates if the robotic errors would have an effect on AM techniques. The speckle correlation sensor is described in section 2 and the AM technique used here, Wire+Arc Additive Manufacture (WAAM), is described in section 3. Finally, in section 4 and 5 the experimental procedure and the results are presented and the compensation strategies are developed and validated the robotic errors by building test parts.

2. <u>Laser speckle correlation sensor</u>

When a laser beam illuminates a rough surface, which has a surface roughness larger than the wavelength, the resulting scattered light intensity distribution shows a granular interference structure which is also known as the laser speckle pattern [6]. These speckle patterns and their evolution in time carry information about the surface properties and deformations. Laser speckle correlation is a measurement philosophy that relates the deformation of an illuminated object to the translation and de-correlation of its observed speckle pattern. The approach was first described in the 1980's by Yamaguchi [7], who applied it to the measurement of object translation, rotation, strain and surface roughness.

More recently, advances in camera and signal processing technology, have made new applications viable and there has been renewed interest in the technique with researchers investigating new applications in industry [8], [9] and at Cranfield University to robotic vehicle odometry [10], [11] and more recently to robotic positioning and stabilisation applications.

The principle of the technique applied to robotic end-effector positioning, is shown in Figure 2. A laser is mounted upon the end-effector and is used to illuminate a region of the workpiece, the resulting scattered light and speckle pattern is then recorded by a camera also mounted on the robot. A sequence of speckle patterns is recorded and analysed as the robot moves above the surface, with the shift of the speckle pattern being related to the relative translation of the robot and workpiece. By continually tracking the motion from the starting position the robots relative position can be found, additionally as the time period between consecutive camera frames is known then robot's instantaneous velocity can be also determined. To determine the shift of the speckle pattern between frames, a 2D cross-correlation is used [12] followed by a peak fitting process to find the shift of the correlation peak from the image centre as shown in Figure 2.
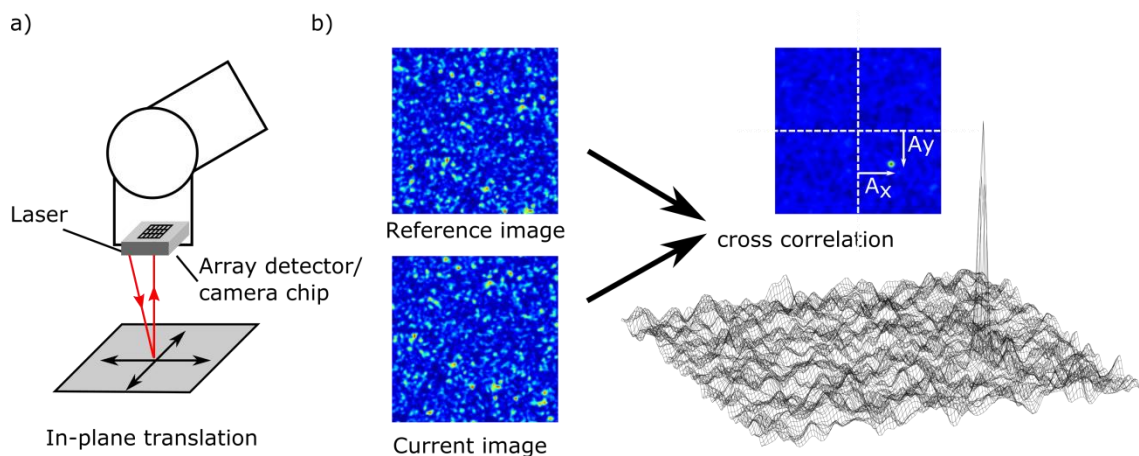

Figure 2 Speckle correlation sensing concept for robotic end-effector sensing

In the Figure 2, it is seen that a laser illuminates the workpiece surface and the resulting speckle patterns are recorded by an array detector/camera. Then the signal processing principle is shown with the cross-correlation of current speckle pattern with a reference pattern calculated (Figure 2). The shift of the resulting peak in the cross-correlation can then be used to determine the robots translation.

The relationship between the speckle pattern shift and the real translation can be described using a series of scaling factors defined as the ratio of pattern shift to surface shift that are dependent on illumination and detector geometry [13], [14]. In this work lens-less or objective speckle patterns are used giving the advantages of better signal levels, a simpler optical configuration, and greater control over the scaling factors via changes to the sensor geometry [11].

The scaling factors for in-plane translations can easily be found by calibration of the sensor on the surface to be measured and generally the technique is robust and tolerant of the surface material with good speckle visible from materials ranging from metals, cardboard to

sand and rocks. However, it is important to note the speckle patterns are also sensitive to any tilting motion between surface and detector planes which may introduce spurious in-plane displacements and appear as apparent translations. Additionally, the surface must be flat as the scaling factors can be shown to be sensitive to the local surface gradient at the illuminated spot [13]. Similarly the surface must be kept at a fixed angle and working distance with respect to the detector, with any changes requiring a recalibration.

The sensor used in this work is shown in Figure 3 The laser source used was an optical fibre coupled diode laser operating at 652 nm with output power of 0.5 mW, with the beam delivered to the sensor via an optical fibre link. At the sensor head the beam exits the delivery fibre and is expanded to a 10 mm spot of the surface via a f=50 mm plano-convex lens. The resulting speckle pattern was then recorded by the detector, a Ximea MQ013MG-ON USB 3.0 camera, with a pixel size of 4.8µm. This was set to acquire 512x512 pixel images at a rate of 500 fps and exposure time of 600 µs, with the control, capture and processing performed on a laptop PC at the same rate.

A laser line band-pass filter was mounted in front of the camera to block ambient light. These components were mounted in a custom 3D printed sensor head which was mounted on the robot end-effector as shown in Figure 3.

The signal processing consisted of a 2D cross-correlation followed by sub-pixel peak finding using a three-point Gaussian peak [12]. Once the speckle shift with respect to the reference image has been found, this is converted to a real translation via the pre-calibrated scaling factors and the velocity can be found by differentiation with the previous position.
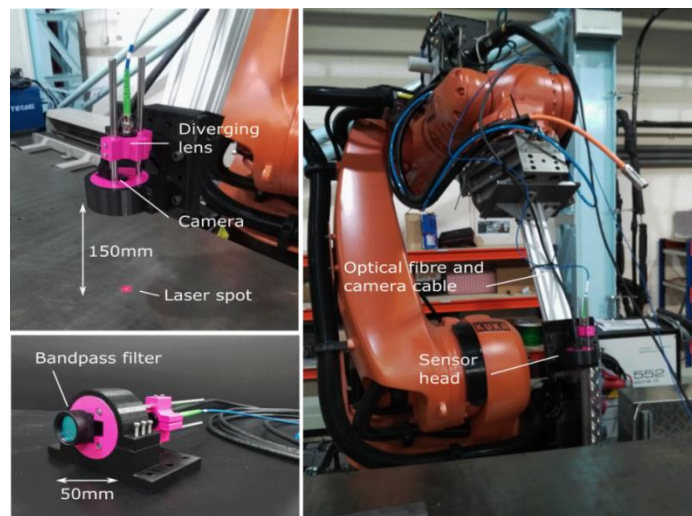

Figure 3 Sensor attachment to KUKA KR150 L110/2 robot

3. WAAM

Wire + Arc Additive Manufacture (WAAM) process is a direct feed processes which uses an arc as the heat source and metallic wire as the feed stock. In the WAAM process, "weld" beads are deposited layer by layer to build 3D components [15]. Standard arc welding process, such as metal inert gas (MIG), tungsten inert gas (TIG), and plasma arc welding (MAT), are applied in the WAAM process. High deposition rates, low material and equipment costs and good structural integrity make WAAM a potentially highly beneficial

replacement for machining parts out of solid billets or forgings [16]. The WAAM system can be easily configured with any industrial robotic systems or gantry systems [3].

WAAM technology substantially slices a 3D model into several 2D features/layers with nominal height (layer height) and the layer height is limited due to the type of the WAAM process [17]. The required layer is built by moving the torch along the tool paths, thus depositing the material in the required places. In order to obtain a geometrically stable deposited product, it is essential to deposit the weld metal using a tool path or strategy which results in a flat surface to be good base for the subsequent layer. Consequently, that would nullify the amplification of distortion, residual stresses, dimensional inaccuracies, weld defects etc. There are different types of tool paths to build a feature and the simplest is a wall. While building wide walls, when the thickness of the wall exceeds the upper limit of the process, the wall is typically divided into several parallel beads also known as parallel building strategy [18]. Figure 4 demonstrates different ways of parallel building strategy.
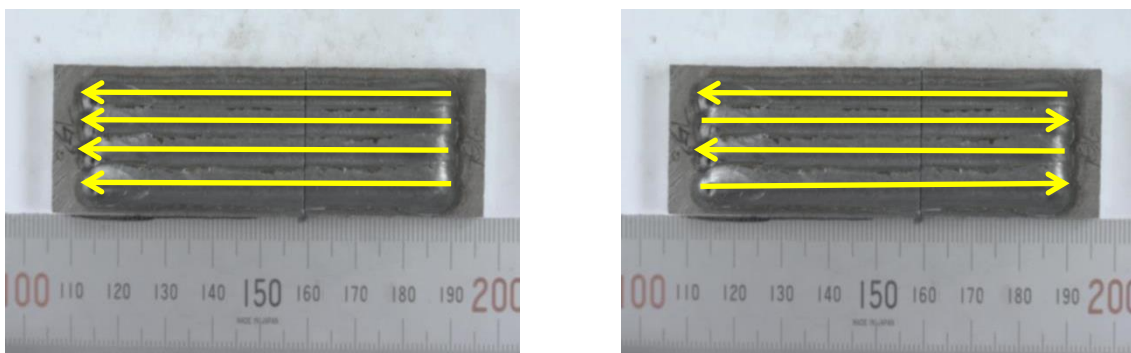

Figure 4 Different ways of parallel building strategy

A group of strategies named Oscillation strategy is one of the deposition patterns, which offers several advantages compared to depositing in a parallel fashion. In this strategy, the deposition of metal is performed in an oscillated manner. Figure 5 describes the different geometric patterns.
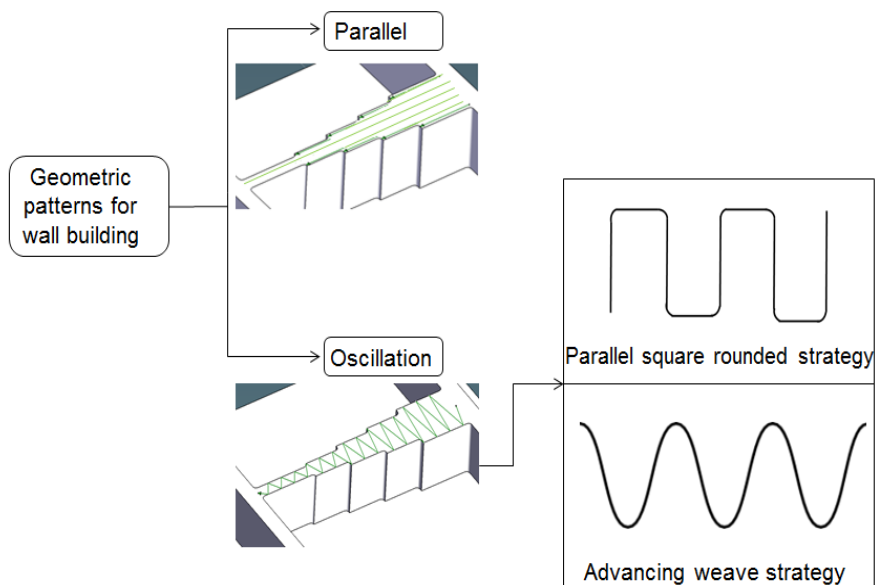

Figure 5 Geometric patterns for part building

The main advantage of the oscillation strategy compared to the parallel is its flexibility to build different wall widths without a continuous change of weld parameters. Thus, oscillation strategy is more accurate in thickness control of the wall. Ultimately, the deposited part will be much closer to the net shape. Moreover, depositing in an oscillated way reduces the probability of producing lack of fusion defects as it a warmer process compared to the parallel strategy. Also, there is no need to turn arc off and on for depositing subsequent passes, thus, fabrication time is reduced when compared to building in parallel strategy.

There are different types of geometric patterns under oscillation strategy, such as but not limited to parallel square rounded pattern, advancing weave strategy. However, in this paper, parallel square oscillation strategy is taken up for the deposition.

Terminology

It is essential to have a consistent terminology associated with the strategy to characterize it. Thus, a terminology is developed to describe the parallel square rounded pattern used shown in figure 6, and is as follows:
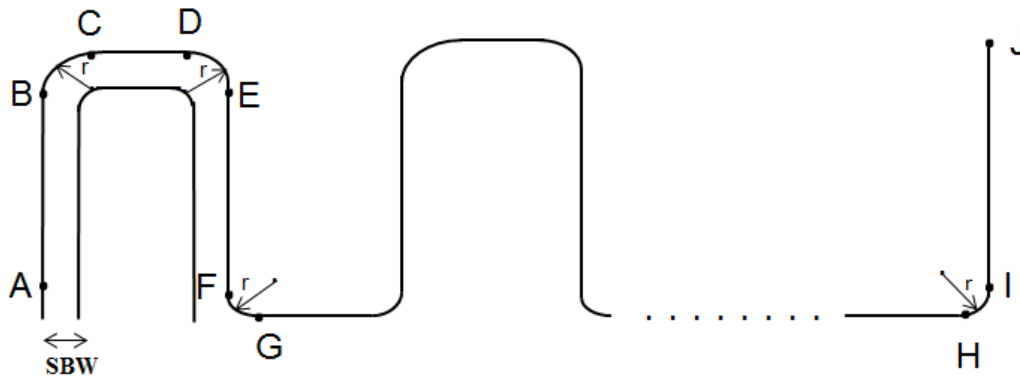

Figure 6 Parallel square rounded pattern

Single bead width (SBW): is the stabilised layer width while building a single pass multi-layer wall, for a particular Wire feed speed (WFS) and Travel speed (TS).

Single bead height (SBH): is the stabilised layer height (out-of-plane in figure 6) while building a single pass multi-layer wall, for a particular WFS and TS.

Corner radius (r): is the radius included in the geometric path to avoid sharp corners.

Oscillation width (o.width): is the distance traversed by the welding torch in the lateral direction. In the **Figure 6**, o.width is EF+2r.

Oscillation layer height (o.height): is the layer height obtained after subsuming with previously deposited metal adjacent to it.

Step advancement (SA): is the distance between two adjacent passes traversed by the welding torch in an oscillation pattern. It is expressed as % of SBW. In the Figure 6, BE represents step-advancement.

4. Experimental Procedure

For the robotic speed measurements, the tool holder of the KUKA robot, which had welding torch mounted on to it, is replaced by a bracket which had the sensor attached to it, as shown in **Error! Reference source not found.**. It was then followed by two calibration stages; the first replaced the sensor with a mounted spike set to the same working distance as the sensor. A standard robot XYZ 4-point tool centre point calibration [19] was then performed to define the TCP to correspond to the laser spot. The spike was then replaced by the sensor head and calibrated by moving the KUKA robot 200 mm in the x and y directions sequentially whilst recording the speckle shifts. The scaling factors were then computed.

The robot is programmed to move in the parallel square rounded oscillation pattern for 100 mm in the longitudinal direction for different oscillations widths, namely 10 mm, 30 mm and 50 mm. Then the robot was programmed to come back to the starting point, wait for 60 seconds and then traverse the same parallel square rounded oscillation pattern with the sensor tracking the position of the robot. This process was then repeated five times to allow an assessment of the repeatability with the sensor acquiring measurements for each path separately.

The velocity components in both X and Y directions, V_x and V_y respectively were then computed by differentiation of the measured robot positions. The final travel speed of the robot is then calculated as:

$$TS = \sqrt{V_x{}^2 + V_y{}^2}$$

In order to know if the robotic velocity errors have an influence on the WAAM build process weld samples with oscillation widths of 10 mm, 30 mm and 50 mm were deposited. The weld investigations were performed on a mild steel plate using the Cold Metal Process (CMT) process with steel solid wire consumable electrode G3Si1. The weld trials were conducted with a KUKA KR150 L110/2 and also on a CNC machine separately. Both of them deployed a Fronius CMT welding power source. Figure 7 shows the set-up. A shielding gas with composition of Argon 80% and CO_2 20% was deployed with a gas flow rate of 15 l/min and a WFS of 4 m/min and Travel speed (TS) of 7 mm/s were used for the deposition. This resulted in spatter free deposition and produced wide and shallow bead with SBW as 4 mm and SBH as 2.5 mm and with a step-advancement of 66% of SBW, which is equal to 2.65 mm.

A program was created to trace the welding torch in the parallel square oscillation pattern (see **Figure 6**). The deposition started at point A and traced along AB, BC, CD and so on, until the torch reached point J along GH, HI and IJ. For the next layer, deposition started at point I and traced along IJ, JG, GH and so on, until the torch reached point B along CD, DA and AB. In total, 5 layers were deposited in alternative deposition directions. The total length of the deposition in longitudinal direction was maintained to be 100 mm. A cooling time of 60 seconds was maintained before depositing the next layer. A corner radius of 1 mm was set in the program to avoid sharp corners. After the deposition, the samples were cut in the lateral direction for the comparison.
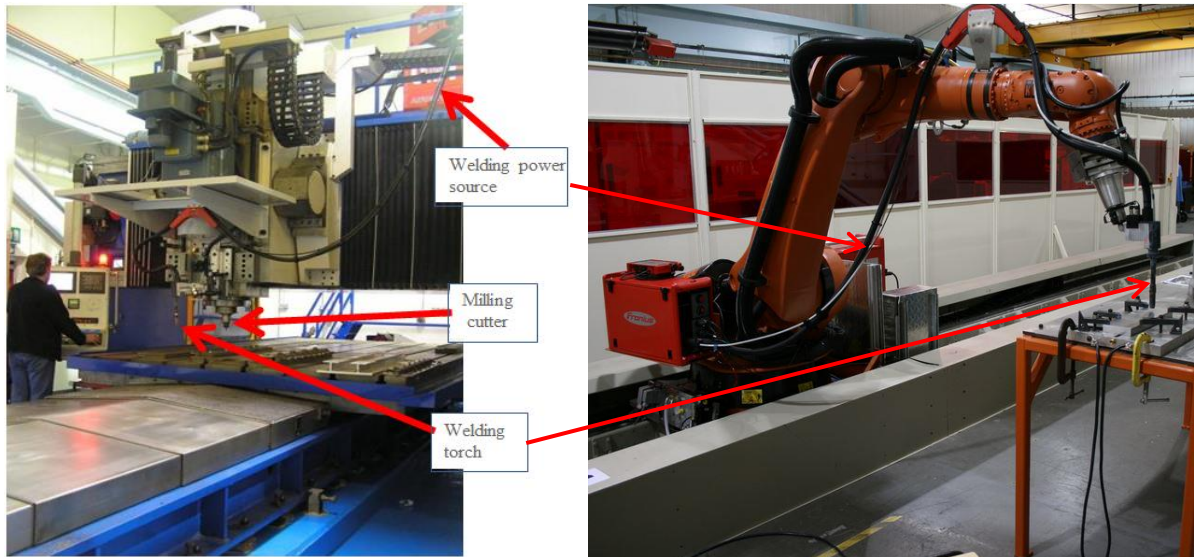
Figure 7 Set up of CNC gantry system (left) and Robotic system (right)

After the weld deposition, the top surface profiles of the deposited samples were measured using an omega portable measuring arm. A laser scanner is used to capture data from the sample's surface. The generated point cloud after scanning is converted to a surface and it is then exported as a CAD file, which can be read in any CAD software and then various characteristics like, but not limited to, surface waviness, top-surface flatness measurements can be measured.

5. RESULTS

i)   Positional Errors

Figure 8 below describes the robotic path movement measured using the speckle correlation sensor for the 50 mm o.width with all the five trials superimposed. From the Figure 8, there are three things which are evident. Firstly, it is seen that all the five trials followed the same path with only small variations of approximately ~10µm between the robotic movements, which proves that the robot maintains its repeatability. In general, the robot's accuracy is largely dependent on the tool path. Less complicated the pattern the more will be closer to the expected destination. Here, the offset of 120 µm very much complies with the robot's position accuracy value mentioned in [20], which is 120 µm. Thirdly, the robot doesn't traverse in an exact circular arc pattern at the edges of the pattern. Since the corner radius is small, it is likely that the robot approximates the circular and straight movement to one single free movement. Similar results with high repeatability and arc patterns were found for other o. widths.
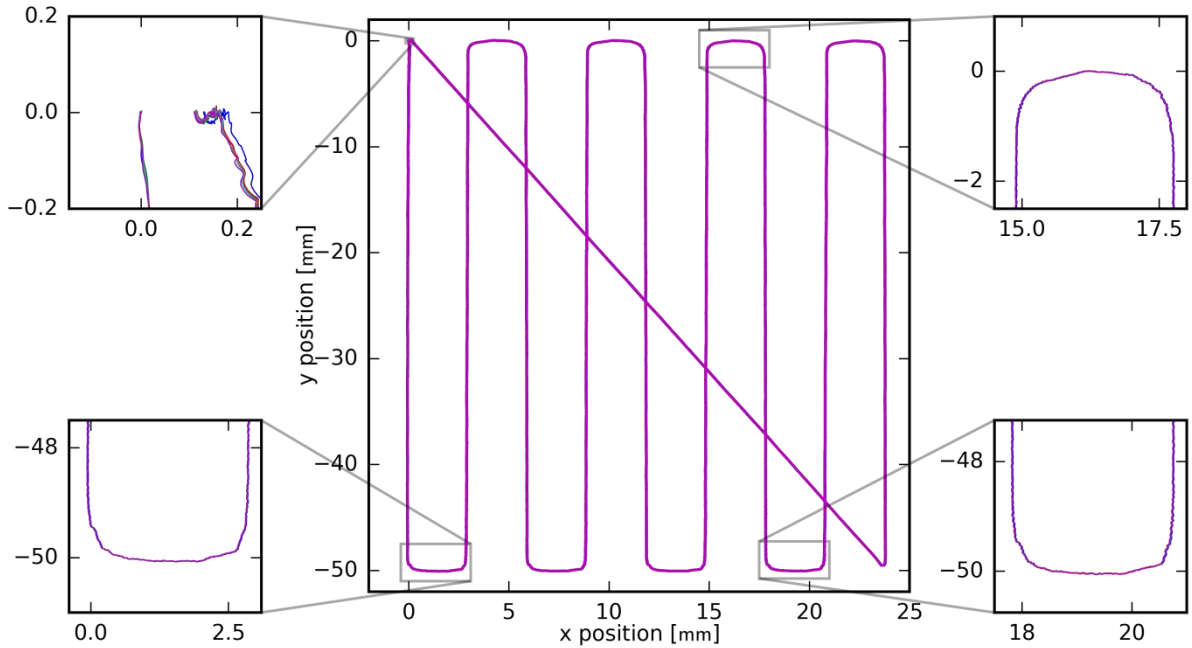
Figure 8 Path traced by the robot for 50 mm o.width, showing 5 overlaid path measurements.

ii)   Tool speed Errors

Figure 9, Figure 10, Figure 11 respectively shows the travel speed profile of the robot, calculated from the position measurements, with respect to time, while traversing 50 mm, 10 mm and 30 mm o.width.

From these travel speed profiles, it is observed that the velocity of the robot throughout the pattern is not constant. It decreases sharply when it reaches the corner radius (shown as point A in figures 9, 10 & 11) and then it increases slightly while traversing the step-advancement (point B) and then decreases when it again reaches the corner radius and finally comes back to original velocity after that traversing the corner radius. The decrease in velocity is nearly same for all the o.widths. The average travel speed at the edges of the pattern comes down to 5.3 mm/s, which is nearly 25 % less than the set travel speed (7 mm/s). This is likely to have an impact in the build quality at the time of deposition due to a change in the amount of material deposited with the change in travel speed occurs at constant WFS.
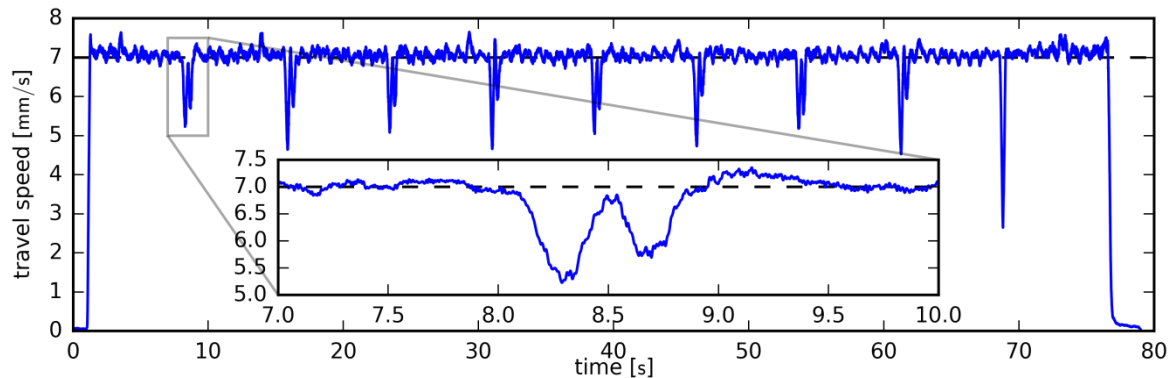

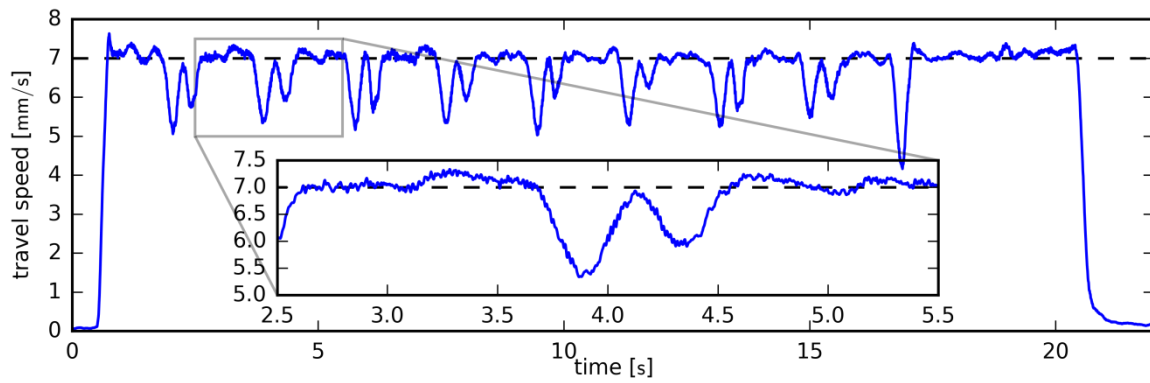**Figure 9** Travel speed profile for 50 mm o.width

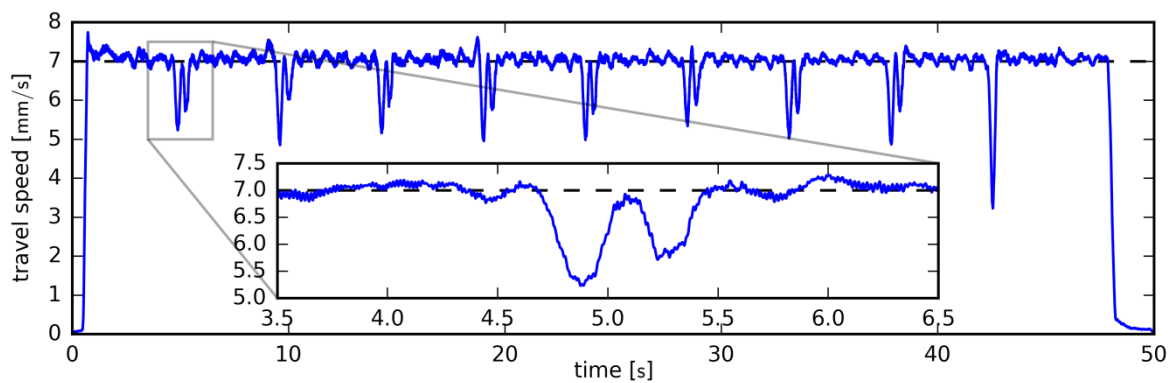**Figure 10** Travel speed profile for 10 mm o.width

Figure 11 Travel speed profile for 30 mm o.width

iii)   Comparison of weld samples deposited with robot and on the CNC machine

To assess the magnitude of this impact on build quality weld samples of 50 mm, 30 mm and 10 mm deposited with the robot and are shown in Figure 12.
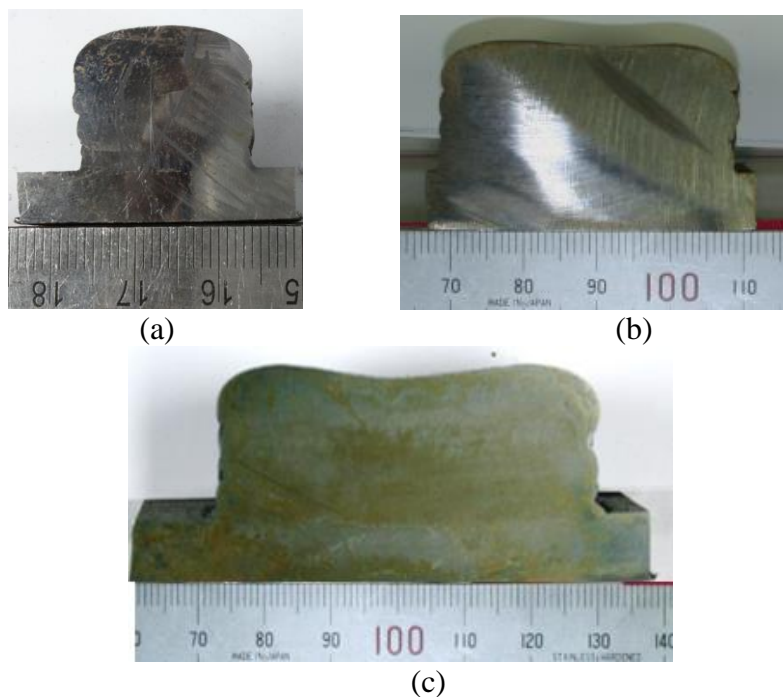

(a)

(b)

(c)

Figure 12 Samples deposited with robot (a) 10 mm (b) 30 mm (c) 50 mm

From the Figure 12, it is clearly seen that the top surfaces are not flat. With an increase in o.width the top surface profile changes from a bulged shape to a U shaped profile. This phenomenon was noticeably increasing with increase in o. width. The reason for this is due to the extra material deposited at the edges of the pattern because of extra path length in the form of step-advancement and also due to the decrease in robot's speed. If the pattern is looked at carefully, see **Figure 6**, the torch was programmed to traverse along the direction of oscillation width, then move in a small circular path with 1 mm radius until it becomes perpendicular to the oscillation width and then it traverses a length measuring step-advancement and subsequently traverses a small circular path of same radius mentioned above until it coincides with the direction of oscillation width. So, during this short time period of traversing along step-advancement, the torch deposits extra weld material, which is not needed for wall building. Thus, the extra material deposited is seen as humps at the edges.

With a decrease in o.width, the two humps get closer and appear to merge together and take the shape of a bulged profile, as seen in the Figure 12 (a). For the 50 mm o.width, after scanning and analysing, it showed a non-uniformity to be nearly 3 mm, after 5 layers, which is the vertical distance between the hump and the height at the centre (Figure 13). This will increase with the number of layers deposited.
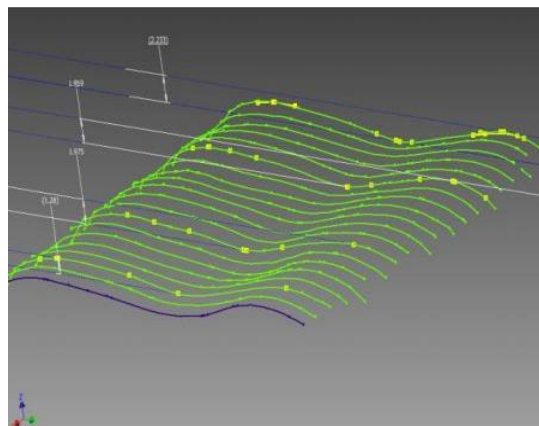

Figure 13 Scanned top surface profile of 50 mm o.width

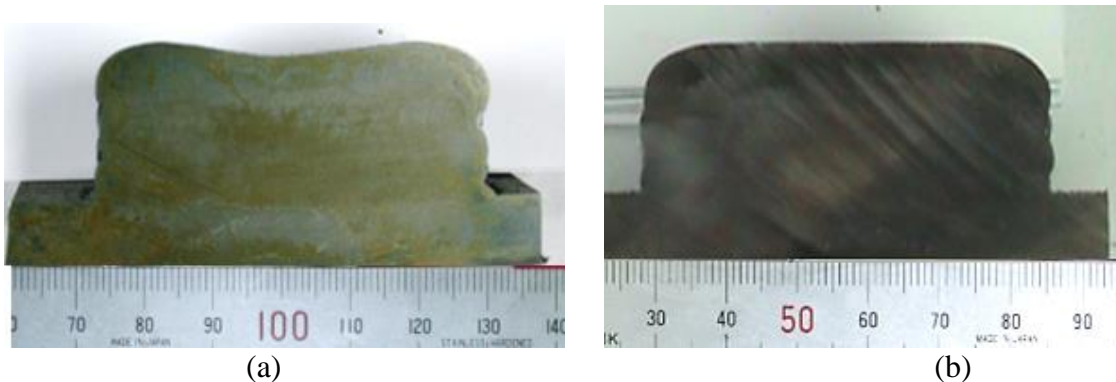Figure 14 shows a comparison between the 50 mm o.width sample built with robot and on the CNC machine.

(a)   (b)

Figure 14 Weld sample deposited on (a) With robot (b) On CNC machine

From the Figure 14, it is seen that the top-surface profile of the sample deposited on CNC machine is better compared to the one deposited using robotic system. This is due to the

fact that, in case of the CNC machine, it is believed that change in speed of the torch is minimal at all points including at the corners of the pattern and thus, the deceleration is also minimal, which means extra metal deposited due to the change in speed of the torch at the corners is also reduced. Therefore, the U shape profile formation is reduced, although there is still the same extra material deposited at the edges of the pattern due to the step-advancement length.

As there is minimal bulging present in figure 14(b), it is clear that the humps at the edges are due to the change in speed of the robot and not due to the step-advancement. The extra material deposited due to step-advancement likely flows in the lateral direction. Probably, this is the reason the o.width measured at the end of the deposition is more than 54 mm which also accounts the half of SBW on either sides of the edges of pattern as well. From the Figure 14 (a), it is seen that the o.width of the sample is slightly more than 54 mm (the 50mm o. width plus 4mm SBW).

iv)   Compensation strategy to counter the build up at the edges

It is very much important to build the weld samples with the top surface as flat as possible. Hence, it is critical to have the same amount of material deposited per unit length across the pattern. The amount of material deposited per unit length is a function of the ratio (WFS/TS). Therefore, at the edges of the pattern, there are two ways to maintain the same amount of material deposited per unit length, which are, either decrease the WFS or increase the TS suitably. However, by increasing TS, it is not completely certain that the robot would decelerate to the speed the user wants. It is also likely that in the due process to maintain the constant speed, the robot might not trace the actual path which is set in the robotic program. Thus, decreasing the WFS is the most viable option.

In this case, since there is a decrease of nearly 25% in TS, WFS is also decreased by the same 25 % at the edges of the pattern i.e. from the point where corner radius starts until the robot traverses the corner radius at the opposite, which also includes traversing the step-advancement. After traversing the corner radius, the WFS is again set to its original value (4 m/min). Figure 15 shows the samples deposited for different o.widths.
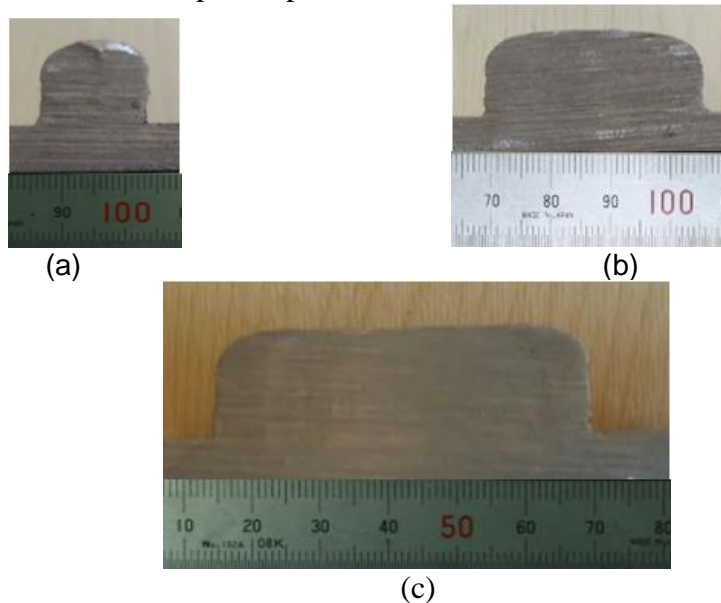

(a)   (b)

(c)

Figure 15 Weld samples after compensation (a) 10 mm (b) 30 mm (c) 50 mm

From the Figure 15, it is clearly seen that the top surface profile of the samples is improved compared to the ones which were built without compensating for the robot's speed errors. It is worth mentioning that due to the decrease in WFS at the edges of the pattern, the extra material deposited while traversing step-advancement is also reduced. The o.width after the deposition is 54 mm for the 50 mm o.width. The layer height at the centre of the welds remains the same as there is no change in weld parameters at the centre and the difference in overall height between the samples with and without compensation at the edges is nearly 3 mm. Overall, the top surface profile is improved.

6. <u>CONCLUSIONS</u>

An assessment has been done as to whether if there are any positional and travel speed errors while traversing a tool path (oscillation strategy) viable for wall building. The positional errors seem to be very much minimal and comply with the robot's specification. However, it was observed from the travel speed profiles that the robot's speed decreased by 25 % at the edges of the pattern. As a result, extra material was deposited at the edges which ultimately made the top surface profile uneven, with vertical bulging of ~3mm after 5 layers observed in build samples. To counter the robotic speed errors, the WFS was also decreased by 25% and the samples built after compensating for the robotic speed errors showed a much improved top surface profile with vertical bulging reduced by 3mm

Additionally, the extra material deposited due to step-advancement stage of the oscillation wall path, causes the measured oscillation width to increase. This is also reduced from 56 mm to 54 mm by the reduction in wire feed speed used to the counter the robotic speed errors.

Irrespective of the additive manufacturing technique, the robotic speed errors are likely to occur and will depend highly upon the tool path applied, hence it is very important to characterise the errors and suitable compensation strategies will have to be incorporated to counter them.

7. <u>REFERENCES</u>

[1]   G. Q. Zhang, X. Li, R. Boca, J. Newkirk, B. Zhang, T. a Fuhlbrigge, H. K. Feng, and N. J. Hunt, "Use of industrial robots in additive manufacturing - A survey and feasibility study," *Proc. Jt. Conf. ISR 2014 - 45th Int. Symp. Robot. Robot. 2014 - 8th Ger. Conf. Robot. ISR/ROBOTIK 2014*, pp. 512–517, 2014.

[2]   Wohlers Associates Inc., "Wohlers Report 2016," 2016.

[3]   Y. Bandari, S. Williams, J. Ding, and F. Martina, "ADDITIVE MANUFACTURE OF LARGE STRUCTURES: ROBOTIC OR CNC SYSTEMS?," in *26th International Solid Freeform Fabrication Symposium, Austin, Texas; 08/2015*, 2015, vol. 1, no. November 2015, pp. 17–25.

[4]   B. Saund and R. DeVlieg, "High accuracy articulated robots with CNC control systems," *SAE Int. J. Aerosp.*, vol. 6, no. 2, pp. 1–6, 2013.

[5]   J. Pandremenos and C. Doukas, "Machining with robots: A critical review," *7th Int. Conf. Digit. Enterp. Technol.*, no. September, 2011.

[6]   J. Dainty, "I The Statistics of Speckle Patterns," in *Progress in Optics*, 1977, pp. 2–46.

[7]   I. Yamaguchi, "Speckle Displacement and Decorrelation in the Diffraction and Image Fields for Small Object Deformation," *Opt. Acta Int. J. Opt.*, vol. 28, no. 10, pp. 1359–1376, Oct. 1981.

[8] M. Farsad, C. Evans, and F. Farahi, "Robust sub-micrometer displacement measurement using dual wavelength speckle correlation," *Opt. Express*, vol. 23, no. 11, p. 14960, 2015.

[9] R. Filter, T. Scharf, and H. P. Herzig, "High resolution displacement detection by speckle pattern analysis : accuracy limits in linear displacement speckle metrology," *J. Eur. Opt. Soc. Rapid Publ.*, vol. 5, p. pp6, Sep. 2010.

[10] T. O. H. Charrett, L. Waugh, and R. P. Tatam, "Speckle velocimetry for high accuracy odometry for a Mars exploration rover," *Meas. Sci. Technol.*, vol. 21, no. 2, p. 025301, 2010.

[11] D. Francis, T. O. H. Charrett, L. Waugh, and R. P. Tatam, "Objective speckle velocimetry for autonomous vehicle odometry.," *Appl. Opt.*, vol. 51, no. 16, pp. 3478–90, Jun. 2012.

[12] M. Raffel, C. E. Willert, S. Wereley, and J. Kompenhans, *Particle Image Velocimetry: a practical guide*. Berlin, Heidelberg: Springer Berlin Heidelberg, 2007.

[13] T. O. H. Charrett and R. P. Tatam, "Objective speckle displacement: an extended theory for the small deformation of shaped objects," *Opt. Express*, vol. 22, no. 21, p. 25466, Oct. 2014.

[14] P. Horváth, M. Hrabovský, and P. Šmíd, "Full theory of speckle displacement and decorrelation in the image field by wave and geometrical descriptions and its application in mechanics," *J. Mod. Opt.*, vol. 51, no. 5, pp. 725–742, Mar. 2004.

[15] J. Ding, F. Martina, and S. Williams, "Production of large metallic components by additive manufacture – issues and achievements," in *1st Metallic Materials and Processes: industrial challenges*, 2015.

[16] S. W. Williams, F. Martina, A. C. Addison, J. Ding, G. Pardal, and P. Colegrove, "Wire+Arc Additive Manufacturing," *Mater. Sci. Technol.*, vol. 23, pp. 73–80, 2015.

[17] F. Martina, J. Mehnen, S. W. Williams, P. Colegrove, and F. Wang, "Investigation of the benefits of plasma deposition for the additive layer manufacture of Ti–6Al–4V," *J. Mater. Process. Technol.*, vol. 212, no. 6, pp. 1377–1386, Jun. 2012.

[18] M. Leinonen, "Additive-Layer-Manufacturing by CMT using Cu97Si3 wire on steel," 2011.

[19] KUKA systems, "KUKA System Software KUKA System Software 8.3 Operating and Programming Instructions for End Users," 2013.

[20] KUKA systems, "Series 2000 : The all-rounders in the high payload range KR 210-2," 2000.

Compensation strategies for robotic motion errors for additive manufacturing (AM)

Bandari, Yashwanth K.

2016-08-10